Dalton Transactions

ROYAL SOCIETY OF CHEMISTRY

PAPER

View Article Online
View Journal | View Issue

Check for updates

Cite this: *Dalton Trans.*, 2021, **50**, 16670

Reduced quenching effect of pyridine ligands in highly luminescent Ln(III) complexes: the role of tertiary amide linkers†

Daniel Kocsi, Daniel Kovacs, Jordann A. L. Wells and K. Eszter Borbas *

Received 28th August 2021,
Accepted 26th October 2021

DOI: 10.1039/d1dt02893f

rsc.li/dalton

Luminescent Eu(III) and Tb(III) complexes were synthesised from octadentate ligands carrying various carbostyril sensitizing antennae and two bidentate picolinate donors. Antennae were connected to the metal binding site *via* tertiary amide linkers. Antennae and donors were assembled on a 1,4,7-triazacyclononane (tacn) platform. Solution- and solid-state structures were comparable to those of previously reported complexes with tacn architectures, with nine-coordinate distorted tricapped trigonal prismatic Ln(III) centres, and distinct from those based on 1,4,7,10-tetraazacyclododecane (cyclen) macrocycles. In contrast, the photophysical properties of these tertiary amide tacn-based complexes were more comparable to those of previously reported systems with cyclen ligands, showing efficient Eu(III) and Tb(III) luminescence. This represents an improvement over secondary amide-linked analogues, and is due to a greatly increased sensitization efficiency in the tertiary amide-linked complexes. Tertiary amide-linked Eu(III) and Tb(III) emitters were more photostable than their secondary amide-linked analogues due to the suppression of photoinduced electron transfer and back energy transfer.

Introduction

The luminescent properties of trivalent lanthanide ions (Ln) have long attracted attention due to their applications in lasers and lighting, encryption, barcoding, and as biological probes. Unlike organic fluorophores that often suffer from short emission lifetimes, broad emission bands, and small Stokes shifts, Ln luminescence is due to f–f transitions, and is therefore atomic-like, unique to the metal, and long-lived.[1,2] The inefficient absorption of Ln(III) centres can be overcome by allowing a light-harvesting antenna to absorb the excitation energy and transfer it to the metal ion. In addition to a high apparent absorption coefficient, such a strategy also yields a large apparent Stokes shift. A dazzling variety of antennae have been reported that encompass amino acids,[3,4] both small and complex heterocycles[5–21] transition metal complexes,[22–29] and even other Lns.[3,30]

A crucial component of an emissive Ln coordination compound is the ligand. Stable complexes require the saturation of most of the 8–10 coordination sites of the Ln(III).[31] Hepta-, octa-, and nonadentate ligands can be constructed from tetra- and triazamacrocyclic (cyclen and tacn, respectively, Fig. 1) building blocks upon the addition of mono- and bidentate donors, *e.g.* carboxylates, carbamides, or picolinates.[32] While the primary role of the ligand is to create a well-defined, stable emitter, it has additional functions. Ln(III) luminescence is sensitive to nearby X–H oscillators.[3,33] While X can be O, N or, in the case of near infrared emitters, even C, the largest quenching effect is due to inner-sphere O–H-containing solvent molecules, such as water or MeOH.[34,35] A high-denticity ligand can displace most inner-sphere solvent molecules, and thus improve Ln(III) luminescence.

A further role of the ligand is to impose a coordination geometry. The shielded 4f-orbitals do not participate in directional bonding, and Lns bind preferentially hard donor atoms (such as O, F) through coulombic interactions. The ligand can thus determine the symmetry around the Ln(III), which in turn will govern the radiative lifetime (τ_{rad}) of the ion. The overall luminescence quantum yield (Φ_{Ln}) is the product of the efficiency with which the Ln(III) excited state is populated (η_{sens}) *via* absorption, intersystem crossing, energy transfer, *etc.*, and the intrinsic quantum yield (Φ_{Ln}^{Ln}) of the ion (eqn (1)). The latter is equal to the proportion of observed (τ_{obs}) and radiative lifetimes.[36,37] All else being equal, shorter τ_{rad} yields higher Φ_{Ln}.

$$\Phi_{Ln} = \eta_{sens} \cdot \Phi_{Ln}^{Ln} = \eta_{sens} \cdot \frac{\tau_{obs}}{\tau_{rad}} \quad (1)$$

Department of Chemistry, Ångström Laboratory, Box 523, Uppsala University, 75120 Uppsala, Sweden. E-mail: eszter.borbas@kemi.uu.se

†Electronic supplementary information (ESI) available: Experimental details, synthesis and chemical characterisation of new compounds, additional photophysical and crystallographic characterization, ^{1}H, ^{13}C, and ^{19}F NMR spectra of new compounds. CCDC 2102702, 2102703. For ESI and crystallographic data in CIF or other electronic format see DOI: 10.1039/d1dt02893f

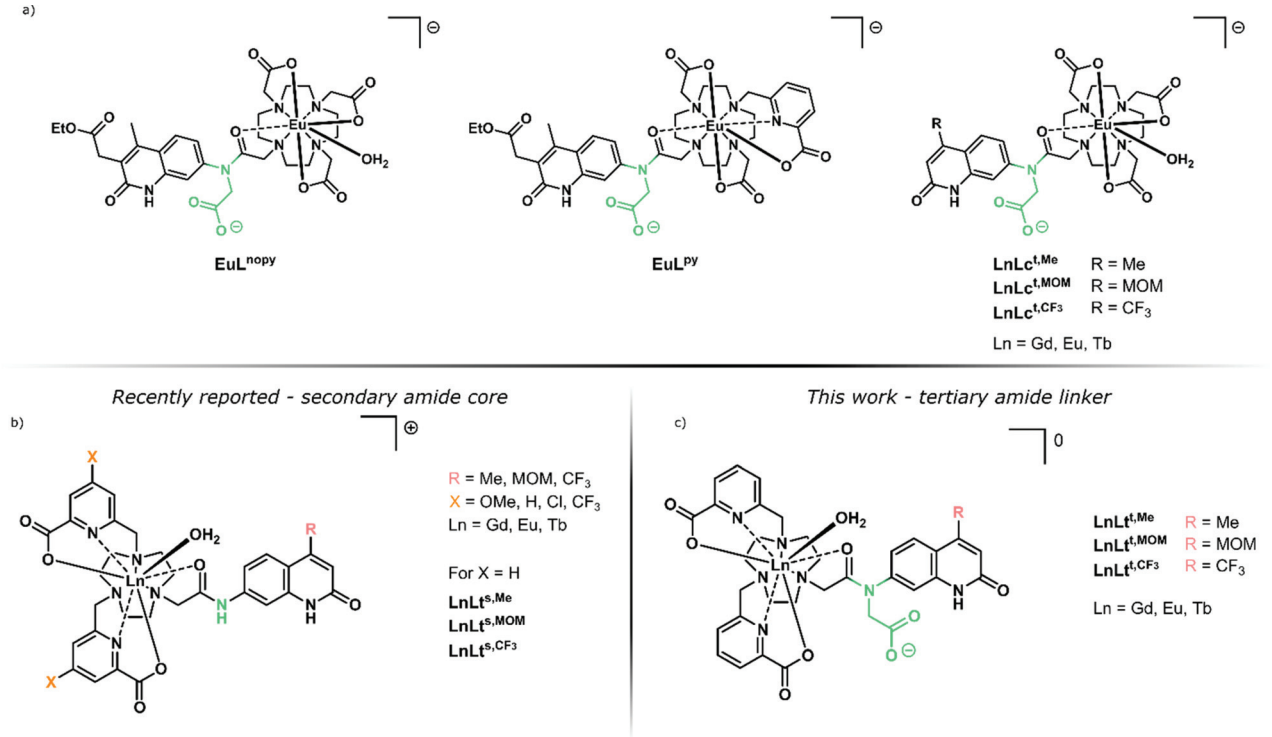

Fig. 1 (a) Previously reported tertiary amide-linked complexes with carbostyril antennae,[39] including cyclen-based benchmarks $\mathbf{LnLc^{t,R}}$.[42] (b) Secondary amide-linked carbostyril-sensitised $\mathbf{LnLt^{s,R}}$ consisting of a tacn ligand framework equipped with substituted picolinic acid donors.[38] (c) $\mathbf{LnLt^{t,R}}$ complexes studied here.

We have previously prepared both tacn and cyclen-based complexes with a variety of carbostyril and coumarin antennae (Fig. 1). Notably, the Eu(III) complexes of the octadentate tacn-based ligands ($\mathbf{LnLt^{s,R}}$) had much shorter τ_{rad} (~3 ms)[38] than those of their similarly octadentate cyclen-based analogues (*e.g.* $\mathbf{LnLc^{s,R}}$, $\tau_{rad} \sim 5$ ms).[39–42]

Ligands can control quenching processes other than X–H quenching. Photoinduced electron transfer (PeT) whereby the excited antenna reduces Ln(III) to Ln(II) is common in emitters with reducible Ln(III), such as Eu.[43,44] The re-oxidation of Eu(II) usually yields a quenched complex, although exceptions are known.[45,46] The detrimental effects of PeT in some systems is comparable to that of X–H oscillators.[40] Ligands that stabilise the Eu(III) oxidation state can increase the luminescence quantum yield.[40] The ligand may also directly quench the excited antenna.[39] This is the case in the picolinate-equipped $\mathbf{LnLt^{s,R}}$ (Fig. 1), where the electron-poor pyridines are reduced alongside Eu(III) by the photoexcited antenna. PeT to the pyridines was possible even in the non redox-active Tb(III) and Gd(III), and was more prominent for electron-poor pyridines.[38]

Here, we report a series of tacn-based ligands and their Ln(III) complexes equipped with the same picolinate ligands that were previously shown to be detrimental to Ln(III) luminescence (Fig. 1). We show that changing the linker that connects the carbostyril antenna to the tacn fragment from a secondary ($\mathbf{LnLt^{s,R}}$) to a tertiary amide ($\mathbf{LnLt^{t,R}}$) can result in the recovery of Ln(III) luminescence, and afford emitters that are comparable to what was seen in cyclen-based systems. The complexes were structurally characterised by paramagnetic ^{1}H NMR spectroscopy and X-ray crystallography to enable comparison of the Ln(III) coordination environments in the secondary and tertiary amide-linked complexes. Steady-state and time-resolved luminescence spectroscopy was used to understand the sensitization and quenching pathways in these emitters, and revealed a significantly improved sensitization in the new set of picolinate-containing species compared to the previously reported ones. These results indicate that even efficient quenching processes can be interrupted by judiciously chosen structural changes.

Results and discussion

Synthetic procedures

The ligands $\mathbf{Lt^{t,R}}$ were synthesised from 4-methyl-, 4-methoxymethyl- or 4-trifluoromethyl-substituted 7-aminocarbostyrils **1a**, **1b** and **1c**, *via* the tertiary chloroacetylamides **2a**, **2b**, and **2c**, respectively (Scheme 1). The latter were prepared similarly to their *tert*-butyl ester analogues.[38] Di-substituted triazanonane **3** was monoalkylated with **2a–c** to yield protected ligands **4a–c**, which were deprotected under basic conditions. Heating $\mathbf{Lt^{t,R}}$ with $LnCl_3$ in a warm EtOH : H_2O mixture yielded $\mathbf{LnLt^{t,R}}$ after column chromatography on silica gel using ^{i}PrOH : H_2O as the eluent in quantitative yield as white solids. Detailed

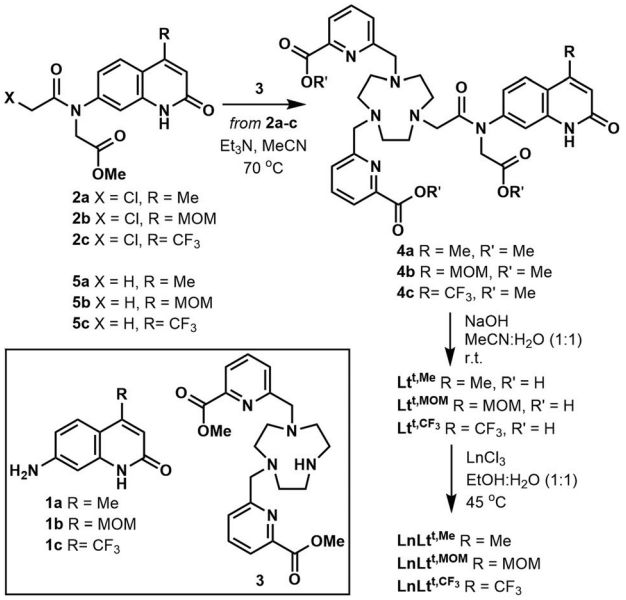

Scheme 1 Preparation of $LnLt^{t,R}$ and model compounds **5a–c**.

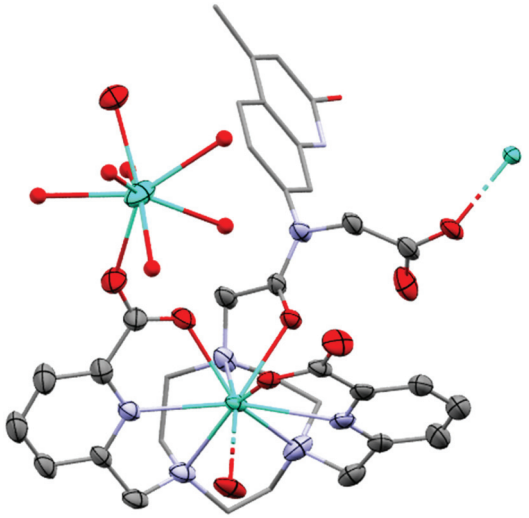

Fig. 2 Solid-state structures of $TbLt^{t,Me}$. H atoms, non-coordinating Cl^- counterions and water molecules omitted, triazacyclonane C atoms and antenna displayed as capped sticks and Ln2 co-ligands displayed as ball and stick for clarity. Ellipsoids displayed at 35% probability. Only major component of disordered sites displayed.

experimental procedures and full chemical characterization for all new compounds are given in the ESI.†

X-ray crystallography

Single crystals suitable for X-ray diffraction analysis were obtained by vapor diffusion of glyme into concentrated aqueous solutions of $GdLt^{t,Me}$ and $TbLt^{t,Me}$. The presence of the carboxylate group on the amide functionality of the ligand results in a coordination motif not seen for related complexes containing secondary amides.[38] The carboxylate group acts as a bridging ligand between **LnLt** molecules, forming 1D-polymeric chains. In addition, a secondary Ln centre is coordinated to a pyridine carboxylate C=O bond, acting as a bridge between 1D-polymeric chains resulting in a 2D-polymeric network (Fig. 2).

The Ln centre within the macrocylic cavity exhibits a nine-coordinate distorted tricapped trigonal prismatic geometry, comparable to that observed in related complexes. The trigonal prism is represented by three tacn N-donor atoms (N_{3PL}), and two pyridine N- and the antenna amide O-atoms (NNO_{PL}). The pyridine carboxylate groups and the bridging carboxylate arm of the tertiary amide serve as the capping ligands of the trigonal prism. The angle between the two planes is 115.1(3)° in Gd and 116.8(6)° in Tb, which compares well to those of related complexes. The deviation of the angle from 180° can be ascribed to the highly distorted geometry of the metal centre. The distance between the Ln centres and the NNO_{PL} are comparable to those of the corresponding secondary amide complexes (0.312(3) and 0.328(6) Å for Gd and Tb, respectively, *versus* average 0.312 Å), as are the distances to the N_{3PL} (Gd: 2.044(3) Å; Tb: 2.024(8) Å; *versus* 2.046 Å average). These metrics suggest that the tertiary amide group and the carboxylate bridging ligand have no significant impact on the direct coordination sphere of carbostyril-substituted tacn systems. The complexes are racemic in the solid-state with both Δ and Λ isomers present in the unit cell. The Ln–O (Gd: 2.388(4) Å; Tb: 2.376(6) Å), tacn Ln–N (Gd: 2.646(4) Å; Tb: 2.64(1) Å) and pyridine Ln–N (Gd: 2.548(6) Å; Tb: 2.538(8) Å) bond distances compare well to those of related complexes.

The secondary Ln centre is eight-coordinate and exhibits a square antiprismatic arrangement. Two picolinate carbonyl groups occupy flanking positions, while the remaining six sites are occupied by water ligands, and the charge balancing chloride counter-ions are non-coordinated and reside in the crystal lattice. The metal centre at this position is partially occupied (75%), which results in considerably disordered lanthanide bound ligands and imprecise bond lengths, which are not discussed here (see ESI† for further information).

NMR studies

Paramagnetic ^1H and ^{19}F NMR spectroscopic analysis of $EuLt^s$ and $EuLt^t$ was performed in D_2O. Complexes with identical metal-binding sites had similar spectra (Fig. 3). At r.t. the signals were broad and indicative of the presence of several species that made the comparison of the data difficult. However, good quality spectra were obtained in all cases upon heating the samples at 80 °C. At high temperature the ^1H NMR spectra of the $EuLt^s$ species contained ~15 signals, consistent with the presence of a single species or of several species rapidly interconverting on the NMR timescale (Fig. S3–18†). The spectra of $EuLt^t$ were much sharper than those of the corresponding $EuLt^s$ even at room temperature, and further improved upon heating. The 80 °C-spectra of $EuLt^t$ contained two sets of signals, which suggests that there are two stable conformers in the solution even at high temperatures. These

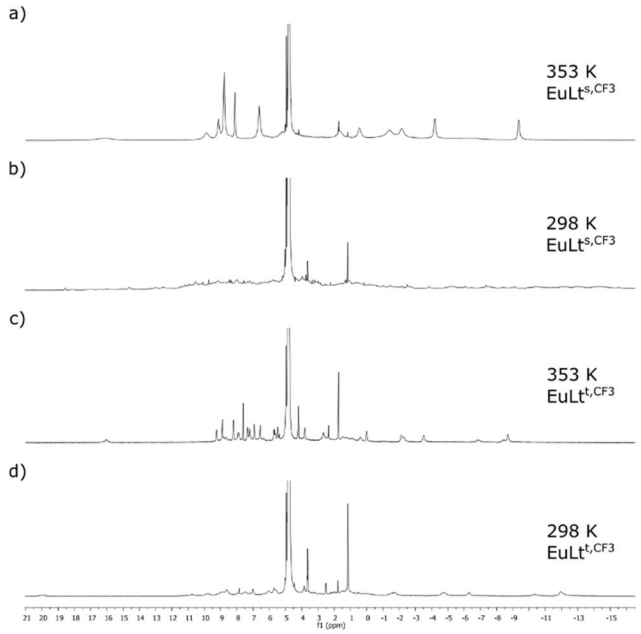

Fig. 3 Variable temperature ^{1}H NMR spectra recorded in D_2O. (a) **EuLt^{s,CF3}** at 353 K. (b) **EuLt^{s,CF3}** at 298 K. (c) **EuLt^{t,CF3}** at 353 K. (d) **EuLt^{t,CF3}** at 298 K.

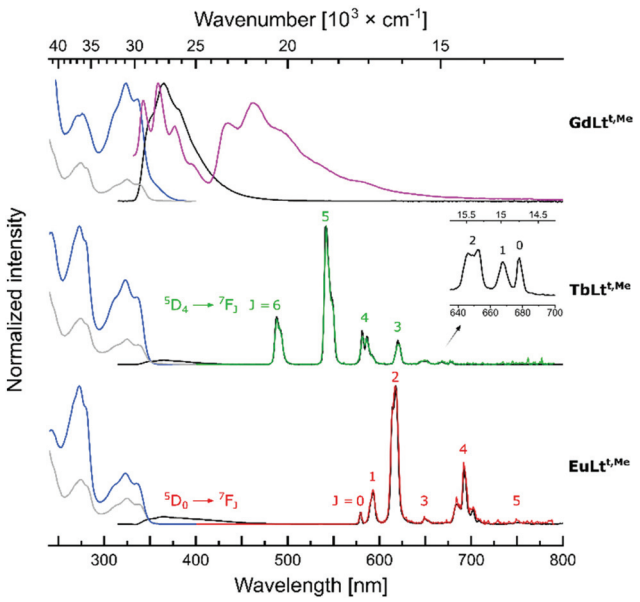

Fig. 4 Normalised absorption (left, grey). Excitation [left, blue, λ_{em} = 405 nm (Gd), λ_{em} = 542 nm (Tb), λ_{em} = 618 nm (Eu), 298 K], steady-state emission (middle, black, λ_{ex} = 325 nm, 298 K), steady-state emission [middle, purple, λ_{ex} = 325 nm (Gd), 77 K] and time-resolved emission (right, green (Tb), red (Eu), λ_{ex} = 325 nm) spectra of **LnLt^{t,Me}** complexes.

conclusions were supported by the ^{19}F NMR analysis of **EuLt^{s,CF3}** and **EuLt^{t,CF3}**. At r.t. a large number of signals were observed for **EuLt^{s,CF3}**, and a broadened peak consisting of several peaks for **EuLt^{t,CF3}**. In line with the ^{1}H NMR data, at 80 °C the signals collapsed into a single peak (−61.9 ppm), while that of **EuLt^{t,CF3}** into one major and two minor ones (around −62.7 ppm) (Fig. S11–18†).

Photophysical studies

The photophysical properties of **LnLt^{t,R}** were measured under the same conditions as those of **LnLt^{s,R}** and **LnLc^{t,R}**,[38,42] in PIPES-buffered pH = 6.5 aqueous solution at r. t. The **LnLt^{t,R}** absorption spectra contained peaks in the 250–310 nm region that were absent from the spectra of **LnLc^{t,R}**, but were present in **LnLt^{s,R}** (Fig. 4, S22–27†). These peaks were assigned to pyridine π–π* transitions. The longest-wavelength absorption was determined by the antenna (Table 1), and the position of the maxima increased in the order **LnLt^{t,Me}** (λ_{abs} = 325 nm) < **LnLt^{t,MOM}** (λ_{abs} = 328 nm) < **LnLt^{t,CF3}** (λ_{abs} = 338 nm). Upon antenna excitation weak antenna fluorescence was observed at λ_{em} = 366–391 nm; longer emission wavelengths were seen for the more red-absorbing antennae. While λ_{abs} for **LnLt^{t,R}** were at wavelengths that were 3–4 nm shorter than seen for the corresponding **LnLt^{s,R}**, this small difference all but disappeared in the emission spectra.

The antenna first triplet excited states (T_1) were determined from the 0–0 transitions of the low-temperature fluorescence spectra (Table 1). The differences between the secondary and tertiary amide-linked antennae are small. The former are lower in energy, but only by 100–300 cm^{-1}. Oxygen sensitivity due to

Table 1 Antenna photophysical properties of **LnLt^{s,R}** and **LnLt^{t,R}**[a]

Compound	λ_{max} [nm]	λ_{em}[b] [nm]	$E_{00}(S_1)$[c] [cm^{-1}]	$E_{00}(T_1)$[c] [cm^{-1}]
GdLt^{s,Me}	329	366	28 900	22 900
GdLt^{t,Me}	325	365	29 200	23 000
GdLt^{s,MOM}	331	376	28 500	22 500
GdLt^{t,MOM}	328	375	28 900	22 800
GdLt^{s,CF3}	342	391	27 400	21 700
GdLt^{t,CF3}	338	391	27 500	22 000

[a] In aqueous PIPES buffer (10 mM), pH 6.5, at 10 μM complex concentrations. [b] λ_{ex} = 329 nm (**GdLt^{s,Me}**), 325 nm (**GdLt^{t,Me}**), 335 nm (**GdLt^{s,MOM}**), 328 nm (**GdLt^{t,MOM}**), 331 nm (**GdLt^{s,CF3}**), 330 nm (**GdLt^{t,CF3}**). [c] Calculated from the 0–0 transitions of the Gd-complexes recorded at 77 K.

back energy transfer (BET) was previously seen in **LnLt^{s,CF3}**.[42] To avoid BET the antenna T_1 should be at least 2000 cm^{-1} above the Tb(III) excited state (20 400 cm^{-1}).[32,47] The 300 cm^{-1} increase in T_1 energy to 22 000 cm^{-1} in **LnLt^{t,CF3}** is probably not sufficient to prevent BET.

Emission spectra were collected with λ_{ex} > 325 nm to avoid excitation of the pyridines. Antenna excitation yielded Tb(III) and Eu(III) emission from all the complexes. Spectral shapes and the ratios of peak intensities were similar in **LnLt^{s,R}** and **LnLt^{t,R}**, but differed from those observed in cyclen-based **LnLc^{t,R}** (Fig. S29–40†). Thus, **LnLt^{s,R}** and **LnLt^{t,R}** have similar coordination environments, which differ from that created by the DO3A-type ligands. As in the cyclen-based systems,[42] the influence of the linkers on the coordination geometry is negligible. The Tb(III) and Eu(III) spectra consisted of 6 and 5 major

signals corresponding to the $^5D_4 \rightarrow {}^7F_J$ (J = 6–0) the $^5D_0 \rightarrow {}^7F_J$ (J = 0–5) transitions, located at 488, 543, 582, 620, 652, 668, and 678 nm, and at 579, 593, 614, 649, 693, and 751 nm, respectively (Fig. 4).

The antenna and Ln(III)-based luminescence quantum yields (Φ_L and Φ_{Ln}, respectively) were determined by the optically dilute method using quinine sulfate (QS, Φ = 0.59)[48] as the external standard (Table 2). Gratifyingly, Φ_{Ln} obtained for the current series of Eu(III) and Tb(III) emitters (**LnLt^{t,R}**) were comparable to the high values previously obtained for the *tert*-amide-linked DO3A-based species (**LnLc^{t,R}**), a major improvement over the weak emission of **LnLt^{s,R}**. The highest Φ_{Tb} and Φ_{Eu} were measured for **TbLt^{t,MOM}** (42%) and **EuLt^{t,CF3}** (13%), respectively. As before, Φ_L were low, below 7% in all cases. Intriguingly, there was no discernable pattern as to the order of Φ_L in the different ligand frameworks. In the non-photoactive and non-redox-active Gd(III) species, Φ_L decreases as follows: **Lc^{t,Me}** > **Lt^{t,Me}** > **Lt^{s,Me}**, **Lt^{s,MOM}** > **Lc^{t,MOM}** ≈ **Lt^{t,MOM}**, and **Lt^{s,CF3}** > **Lt^{t,CF3}** ≈ **Lc^{t,CF3}**.

PeT from the antenna to the pyridines and to Eu(III) was calculated to be thermodynamically feasible (eqn (2)). Cyclic voltammetry yielded E_{ox}, the electron donor oxidation potential, as +1.91, +1.94, and +2.20 V (*vs.* NHE) for the antenna models **5a–c** (Scheme 1, Fig. S19–21†), respectively. These models were prepared to enable cyclic voltammetric analysis of the antennae without interference from the other redox-active components of the complexes. E_{red} is the electron acceptor reduction potential. Pyridine E_{red} (−1.29 V *vs.* NHE) has been reported;[38] E_{red} of Eu(III) was approximated with values found for a +1 charged cyclen-based complex (−0.80 V *vs.* NHE for a MOM-substituted complex).[40] This was necessary as the presence of the pyridines, which are reduced at similar potentials make Eu(III) E_{red} determination unreliable in this ligand framework. E_S is the antenna excited state energy, determined from the first vibronic band of the 77 K spectra as 3.60, 3.57, and 3.39 eV for **GdLt^{t,Me}**, **GdLt^{t,MOM}**, and **GdLt^{t,CF3}** respectively. The last term is the coulombic stabilization of the charge-separated system, usually taken as ∼0.15 eV.[49]

$$\Delta G = (E_{ox} - E_{red}) - E_S - \frac{e_0^2}{\varepsilon r} \quad (2)$$

ΔG for PeT from the CF_3-substituted antenna to the pyridine was −0.54 eV. Values for the more electron-rich antennae were more negative, −0.98 eV and −1.04 eV for the MOM- and Me-substituted ones, respectively. Eu(III) reduction was even more favorable, with ΔG values of −0.95, −0.87, and −0.45 eV, for Me-, MOM- and CF_3-substituted complexes, respectively. In DO3A-complexes, *sec*-amide-linked antennae are more fluorescent than the *tert*-amide-linked ones.[42] The overall Φ_L order is the result of the combination of these effects. In the Tb(III) and Eu(III) complexes the situation is further complicated by the photo- and, in the case of Eu(III), redox-activity of the metals.

The number of metal-coordinated water molecules (q) were determined from τ_{obs} of Eu(III) and Tb(III) (Table 3).[3,35] The luminescence decays were monoexponential for these complexes, with τ_{obs} = ∼0.52 ms and ∼1.34 ms for **EuL** and **TbL**, respectively. In all cases q was ∼1, which together with the octadentate ligand gives the expected nine-coordinate complexes. BET in **TbLt^{t,CF3}** did not allow for the determination of q, however, it is most likely 1 by analogy with the other complexes.

The similar Φ_L and Φ_{Ln} values of pyridine-equipped **LnLt^{t,R}** and DO3A-based **LnLc^{t,R}** suggested that either PeT to the pyridines was less efficient in **LnLt^{t,R}** than in **LnLt^{s,R}**, or PET was

Table 2 Antenna- and metal-based luminescence quantum yields of **LnLt^{t,R}**, with comparisons to **LnLt^{s,R}** (Ref. 38) and **LnLc^{t,R}** (Ref. 42). The values in parentheses show the change compared to **LnLc^{t,R}**

Complex	Φ_L [%][a]	Φ_{Ln} [%][a]
GdLt^{s,Me} [b]	4.40 ± 0.10 (63%)	—
GdLt^{t,Me} [b]	5.47 ± 0.07 (79%)	—
GdLc^{t,Me}	6.8 (100%)	—
GdLt^{s,MOM} [b]	6.42 ± 0.28 (131%)	—
GdLt^{t,MOM} [b]	4.94 ± 0.06 (98%)	—
GdLc^{t,MOM}	5.1 (100%)	—
GdLt^{s,CF3} [b]	4.53 ± 0.17 (147%)	—
GdLt^{t,CF3} [b]	3.62 ± 0.02 (113%)	—
GdLc^{t,CF3}	3.2 (100%)	—
TbLt^{s,Me} [b]	3.50 ± 0.10 (58%)	27.05 ± 1.05 (60%)
TbLt^{t,Me} [b]	4.59 ± 0.10 (76%)	40.4 ± 0.40 (93%)
TbLc^{t,Me}	5.9 (100%)	43.4 (100%)
TbLt^{s,MOM} [b]	4.92 ± 0.01 (109%)	28.05 ± 0.95 (64%)
TbLt^{t,MOM} [b]	4.28 ± 0.03 (96%)	41.5 ± 0.50 (93%)
TbLc^{t,MOM}	4.5 (100%)	45.1 (100%)
TbLt^{s,CF3} [b]	4.16 ± 0.24 (142%)	3.24 ± 0.14 (19%)
TbLt^{t,CF3} [b]	3.33 ± 0.28 (116%)	19.0 ± 1.05 (113%)
TbLc^{t,MF3}	3.1 (100%)	15.9 (100%)
EuLt^{s,Me} [c]	0.42 ± 0.03 (29%)	0.83 ± 0.02 (14%)
EuLt^{t,Me} [c]	0.96 ± 0.24 (87%)	3.45 ± 1.10 (83%)
EuLc^{t,Me}	1.5 (100%)	6.0 (100%)
EuLt^{s,MOM} [c]	0.16 ± 0.01 (6%)	2.44 ± 0.07 (28%)
EuLt^{t,MOM} [c]	1.32 ± 0.06 (52%)	5.22 ± 0.15 (61%)
EuLc^{t,MOM}	2.5 (100%)	8.9 (100%)
EuLt^{s,CF3} [c]	0.61 ± 0.02 (23%)	7.95 ± 0.42 (68%)
EuLt^{t,CF3} [c]	2.81 ± 0.08 (100%)	13.0 ± 0.10 (108%)
EuLc^{t,CF3}	2.7 (100%)	11.6 (100%)

[a] Relative to QS (Φ = 0.59) in H_2SO_4 (0.05 M).[48] [b] Mean ± standard deviation for two independent measurements. [c] Mean ± standard deviation for three independent measurements.

Table 3 Ln(III) τ_{obs} and q-values in **EuLt^{t,R}** and **TbLt^{t,R}**[a]

Complex	τ_{H_2O} [ms]	τ_{D_2O} [ms]	q[b]
TbLt^{t,Me}	1.37	2.13	0.99
EuLt^{t,Me}	0.51	1.43	1.18
TbLt^{t,MOM}	1.30	2.01	1.06
EuLt^{t,MOM}	0.52	1.43	1.15
TbLt^{t,CF3}	0.62	1.01	2.71[c]
EuLt^{t,CF3}	0.52	1.43	1.15

[a] Recorded in PIPES-buffered H_2O or D_2O solutions at pH = 6.5 at room temperature. [b] Calculated using q = (5 ms) $(1/\tau_{H_2O} - 1/\tau_{D_2O} - 0.06\ ms^{-1})$ for Tb, and q = (1.2 ms) $(1/\tau_{H_2O} - 1/\tau_{D_2O} - 0.25\ ms^{-1} - m\ 0.075\ ms^{-1})$ for Eu; m = number of nearby amide N–H oscillators.[3,35] [c] Real q value could not be determined.

successfully outcompeted by energy transfer to the Ln(III). The efficiency with which the antenna excited state populates the Ln(III) excited state (η_{sens}) is readily calculated for Eu(III) emitters using eqn (1) and (3) (Table 4).[36,37] Antenna excited state quenching affects η_{sens}. If complexes with identical antennae and similar geometries have different η_{sens}, this difference may be due to differences in PeT. Φ_{Ln}^{Ln} in eqn (1) can be calculated[36] from τ_{rad} of Eu(III), which is obtained from the luminescence spectrum using eqn (3). I_{tot} is the integrated full spectrum (530–800 nm), I_{MD} is the integrated $^5D_0 \rightarrow {}^7F_1$ transition (582–603 nm), $A_{MD,0}$ is the spontaneous emission probability (14.65 s^{-1}), n is the refractive index of the aqueous medium (approximated with water), and τ_{obs} equals τ_{H_2O}.

$$\frac{1}{\tau_{rad}} = A_{MD,0} \cdot n^3 \left(\frac{I_{tot}}{I_{MD}}\right) \quad (3)$$

EuLt^{t,R} and **EuLt^{s,R}** have similar τ_{rad} (~2.9 ms). This is in line with their having similar Ln(III) coordination environments, as suggested by their superimposable luminescence spectra (Fig. S53–55†). The slightly longer τ_{obs} of **EuLt^{t,R}** than of **EuLt^{s,R}** is presumably due to the removal of the N–H group from the amide linker. Overall, the effect of the tertiary amides on Φ_{Ln}^{Ln} is small compared to **EuLt^{s,R}**, and all complexes have $\Phi_{Ln}^{Ln} \sim 17.5\%$. Compared with the $\Phi_{Ln}^{Ln} \sim 12\%$ obtained for **EuLc^{t,R}**, this is a significant improvement. The shortening of τ_{rad} to increase Φ_{Ln}^{Ln} is a rarely used strategy for improving Φ_{Ln}.[50]

Although **EuLt^{t,R}** have higher Φ_{Ln}^{Ln} than **EuLc^{t,R}** their Φ_{Ln} values were similar or lower, due to the lower η_{sens}. **EuLt^{t,R}** shows marked improvement in η_{sens} compared to secondary amide-linked **EuLt^{s,R}** (*e.g.* 28% and 5% in **EuLt^{t,Me}** and **EuLt^{s,Me}**, respectively), just not enough to reach the values seen in **EuLc^{t,R}** (50% in **EuLc^{t,Me}**). The better sensitization in **EuLt^{t,R}** than in **EuLt^{s,R}** may be due to less efficient PeT to the pyridines. This is suggested by the fact that Φ_L in **GdLt^{t,Me}** is somewhat higher than in **GdLt^{s,Me}** even though in DO3A-based complexes secondary amide linked antennae have higher Φ_L than their tertiary amide-linked analogues.[42] However, the low Φ_L values do not allow for a reliable comparison. A second alternative explanation for the observed results may be more efficient energy transfer due to a different antenna orientation. A third possibility is more efficient population of the Ln(III) feeding level, likely the antenna T_1, due to more efficient intersystem crossing in **LnLt^{t,R}** than in **LnLt^{s,R}**. The additional improvement seen in **LnLc^{t,R}** compared to **LnLt^{t,R}** is likely due to the absence of PeT to pyridines. As above, antenna orientation could also play a role. Both **LnLc^{t,R}** and **Lnt^{t,R}** have *tert*-amide-linked antennae, and the similar values of Φ_L are consistent with comparable levels of antenna S_1 quenching. Thus the higher η_{sens} in cyclen-based **LnLc^{t,R}** indicates more efficient energy transfer than in tacn-based **Lnt^{t,R}**.

Photostability of LnL. The photostability of a Ln(III) emitter is an important parameter for practical applications. Unlike those of organic fluorophores, Ln(III) excited states are not sensitive to quenching by atmospheric oxygen.[51] Photodegradation is rather due to processes that compromise the integrity of the other functional units in the complex, often the antenna. BET from Ln(III)* to the antenna T_1 or slow energy transfer from T_1 to Ln(III) caused by too small or too large T_1-Ln(III)* gaps, respectively, both result in long T_1 lifetimes, and thus oxygen-sensitivity.

The photostabilities of the complexes reported herein (**LnLt^{t,R}**) were investigated and compared to those of **LnLt^{s,R}** and **LnLc^{t,R}** (Fig. 5). The Eu(III) complexes proved quite robust, and retained at least 90% of their luminescence after 2.5 h of irradiation. Small differences, however, could be noted.

Table 4 τ_{rad}, Φ_{Ln}^{Ln}, and η_{sens} of EuL

Complex	τ_{rad} [a] [ms]	Φ_{Eu}^{Eu} [b] [%]	η_{sens} [b] [%]
EuLt^{s,Me}	2.87	17.4	5
EuLt^{t,Me}	2.94	17.7	28
EuLc^{t,Me}	5.41	12.0	50
EuLt^{s,MOM}	2.86	17.5	14
EuLt^{t,MOM}	2.96	17.9	30
EuLc^{t,MOM}	5.40	12.2	73
EuLt^{s,CF3}	2.87	17.8	46
EuLt^{t,CF3}	2.99	17.4	75
EuLc^{t,CF3}	5.40	12.2	95

[a] Calculated using eqn (3).[36] [b] Calculated using eqn (1) and (3).[36]

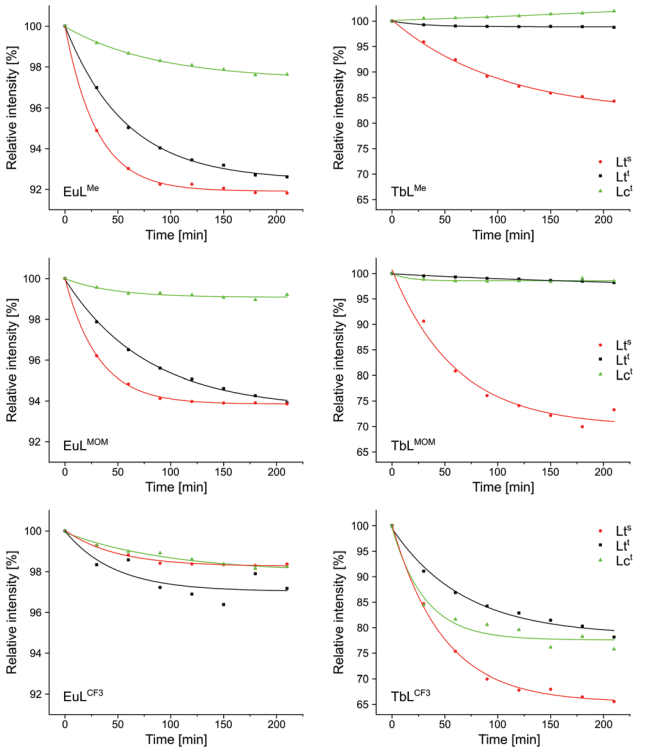

Fig. 5 Photostability of Tb and Eu complexes (10 μM) in aqueous PIPES buffer (10 mM), pH = 6.5, using 395 nm filter for Tb and 500 nm filter for Eu complexes, respectively. λ_{ex}(**LnLc^{t,Me}**) = 324 nm, λ_{ex}(**LnLt^{t,Me}**) = 325 nm, λ_{ex}(**LnLc$^{t,MOM/CF3}$**) = 327 nm, λ_{ex}(**LnLt^{s,Me}**/**LnLt^{t,MOM}**) = 328 nm, λ_{ex}(**LnLt^{s,MOM}**/(**LnLt^{s,CF3}**/**LnLt^{t,CF3}**) = 330 nm. Values normalised to integrated emission intensity at t_0.

Complexes equipped with a CF_3-substituted antenna were the most resistant to photodegradation, while the least stable were the ones carrying the most electron-rich Me-substituted antenna. Cyclen-based **EuLc^{t,R}** were in all cases more stable than their tacn-based analogues **EuLt^{s,R}** and **EuLt^{t,R}**. *Tert*-amide-linked **EuLt^{t,R}** were somewhat more stable then *sec*-amide-linked **EuLt^{s,R}**. These trends are consistent with PeT opening up a degradation pathway for the complex. This pathway is more prominent for picolinate-carrying **EuLt^{s,R}** and **EuLt^{t,R}**, which contain both Eu(III) and pyridines as potential electron acceptors.

In the case of the Tb(III) complexes fastest degradation was seen for those with the lowest antenna T_1. All three CF_3-substituted complexes rapidly lost Tb(III) luminescence efficiency. This loss was fastest for **TbLt^{s,CF3}**, with a sec-amide-linked antenna. For the other two antennae attaching them *via* a *tert*-amide, and the concomitant increase in T_1 was sufficient to protect the integrity of the emitters. These trends indicate that photolability is due to BET populating the antenna T_1, followed by T_1 reacting with atmospheric oxygen.

Conclusions

We investigated the effect of replacing a secondary amide linker with a methylcarboxylate-substituted tertiary amide one on the photophysical properties of tacn-based luminescent Ln(III) complexes. In solution the amide substituent was non-coordinating, and did not alter the coordination geometry of the complex compared to the parent species. This was indicated by the shapes of the Ln(III) luminescence spectra and the radiative lifetimes of the Eu(III) complexes, and was supported by the results of the paramagnetic NMR spectroscopic and single crystal X-ray crystallographic analyses in the solution and solid states, respectively.

Changing the linker from secondary to tertiary amide had a profound effect on the Eu(III) and Tb(III) luminescence. In tacn-based, pyridine-containing Ln(III) complexes with secondary amide linkers pyridine reduction by the photoexcited carbostyril competed efficiently with Eu(III) and Tb(III) sensitization. Upon linker replacement all of the emitters experienced an increase in luminescence quantum yield, with values close to, and in some cases even higher than, those obtained for cyclen-based systems lacking the quenching pyridines. An additional benefit of the *tert*-amide linkers is higher antenna T_1 energy, and thus decreased BET for Tb(III) emitters. Finally, tertiary amide linked complexes based on both tacn and cyclen frameworks showed high photostability, highlighting the importance of closing down PeT and BET quenching pathways to obtain robust emitters.

Author contributions

D. Kocsi and D. Kovacs: conceptualization, resources, investigation, data curation, visualization, formal analysis. J.A.L.W.: investigation, data curation, visualization, formal analysis. K.E. B.: conceptualization, funding acquisition, project administration, resources, formal analysis, visualization, supervision. All authors were involved in the writing of the original draft and took part in the reviewing and editing of the manuscript.

Conflicts of interest

There are no conflicts to declare.

Acknowledgements

This work was supported by the Swedish Research Council (project grant 2017-04077 for K.E.B.), the Knut och Alice Wallenbergs Foundation (Dnr: 2018.0066).

Notes and references

1 J.-C. G. Bünzli and S. V. Eliseeva, in *Lanthanide Luminescence: Photophysical, Analytical and Biological Aspects*, ed. P. Hänninen and H. Härmä, Springer Berlin Heidelberg, Berlin, Heidelberg, 2011, pp. 1–45.
2 A. de Bettencourt-Dias, in *Luminescence of Lanthanide Ions in Coordination Compounds and Nanomaterials*, John Wiley & Sons Ltd, 2014, pp. 1–48.
3 W. D. Horrocks and D. R. Sudnick, *Acc. Chem. Res.*, 1981, **14**, 384–392.
4 W. D. Horrocks, Jr., J. P. Bolender, W. D. Smith and R. M. Supkowski, *J. Am. Chem. Soc.*, 1997, **119**, 5972–5973.
5 A. S. Chauvin, F. Gumy, D. Imbert and J. C. G. Bünzli, *Spectrosc. Lett.*, 2004, **37**, 517–532.
6 A. de Bettencourt-Dias, P. S. Barber and S. Bauer, *J. Am. Chem. Soc.*, 2012, **134**, 6987–6994.
7 A. de Bettencourt-Dias, S. Viswanathan and A. Rollett, *J. Am. Chem. Soc.*, 2007, **129**, 15436–15437.
8 J. H. S. K. Monteiro, A. de Bettencourt-Dias and F. A. Sigoli, *Inorg. Chem.*, 2017, **56**, 709–712.
9 R. Xiong, D. Mara, J. Liu, R. Van Deun and K. E. Borbas, *J. Am. Chem. Soc.*, 2018, **140**, 10975–10979.
10 J. Laakso, G. A. Rosser, C. Szíjjártó, A. Beeby and K. E. Borbas, *Inorg. Chem.*, 2012, **51**, 10366–10374.
11 T. Zhang, X. Zhu, C. C. W. Cheng, W.-M. Kwok, H.-L. Tam, J. Hao, D. W. J. Kwong, W.-K. Wong and K.-L. Wong, *J. Am. Chem. Soc.*, 2011, **133**, 20120–20122.
12 Y. Ning, M. Zhu and J.-L. Zhang, *Coord. Chem. Rev.*, 2019, **399**, 213028.
13 Y. Ning, G.-Q. Jin and J.-L. Zhang, *Acc. Chem. Res.*, 2019, **52**, 2620–2633.
14 Y. Ning, J. Tang, Y.-W. Liu, J. Jing, Y. Sun and J.-L. Zhang, *Chem. Sci.*, 2018, **9**, 3742–3753.
15 D. Parker, P. K. Senanayake and J. A. G. Williams, *J. Chem. Soc., Perkin Trans. 2*, 1998, 2129–2139.
16 A. Beeby, S. Faulkner, D. Parker and J. A. G. Williams, *J. Chem. Soc., Perkin Trans. 2*, 2001, 1268–1273.

17 D. G. Smith, R. Pal and D. Parker, *Chem. – Eur. J.*, 2012, **18**, 11604–11613.
18 D. G. Smith, B. K. McMahon, R. Pal and D. Parker, *Chem. Commun.*, 2012, **48**, 8520–8522.
19 A. Foucault-Collet, C. M. Shade, I. Nazarenko, S. Petoud and S. V. Eliseeva, *Angew. Chem., Int. Ed.*, 2014, **53**, 2927–2930.
20 S. Petoud, G. Muller, E. G. Moore, J. Xu, J. Sokolnicki, J. P. Riehl, U. N. Le, S. M. Cohen and K. N. Raymond, *J. Am. Chem. Soc.*, 2007, **129**, 77–83.
21 S. Faulkner, M.-C. Carrie, S. J. A. Pope, J. Squire, A. Beeby and P. G. Sammes, *Dalton Trans.*, 2004, 1405–1409.
22 C. Y. Chow, S. V. Eliseeva, E. R. Trivedi, T. N. Nguyen, J. W. Kampf, S. Petoud and V. L. Pecoraro, *J. Am. Chem. Soc.*, 2016, **138**, 5100–5109.
23 E. R. Trivedi, S. V. Eliseeva, J. Jankolovits, M. M. Olmstead, S. Petoud and V. L. Pecoraro, *J. Am. Chem. Soc.*, 2014, **136**, 1526–1534.
24 T. N. Nguyen, C. Y. Chow, S. V. Eliseeva, E. R. Trivedi, J. W. Kampf, I. Martinic, S. Petoud and V. L. Pecoraro, *Chem. – Eur. J.*, 2018, **24**, 1031–1035.
25 T. Lazarides, D. Sykes, S. Faulkner, A. Barbieri and M. D. Ward, *Chem. – Eur. J.*, 2008, **14**, 9389–9399.
26 T. Lazarides, N. M. Tart, D. Sykes, S. Faulkner, A. Barbieri and M. D. Ward, *Dalton Trans.*, 2009, 3971–3979.
27 N. M. Shavaleev, L. P. Moorcraft, S. J. A. Pope, Z. R. Bell, S. Faulkner and M. D. Ward, *Chem. Commun.*, 2003, 1134–1135.
28 N. M. Shavaleev, L. P. Moorcraft, S. J. A. Pope, Z. R. Bell, S. Faulkner and M. D. Ward, *Chem. – Eur. J.*, 2003, **9**, 5283–5291.
29 S. J. A. Pope, B. J. Coe and S. Faulkner, *Chem. Commun.*, 2004, 1550–1551.
30 S. Faulkner and S. J. A. Pope, *J. Am. Chem. Soc.*, 2003, **125**, 10526–10527.
31 S. Cotton, in *Lanthanide and Actinide Chemistry*, 2006, pp. 35–60.
32 D. Parker, R. S. Dickins, H. Puschmann, C. Crossland and J. A. K. Howard, *Chem. Rev.*, 2002, **102**, 1977–2010.
33 W. D. Horrocks, Jr. and D. R. Sudnick, *J. Am. Chem. Soc.*, 1979, **101**, 334–340.
34 R. S. Dickins, D. Parker, A. S. de Sousa and J. A. G. Williams, *Chem. Commun.*, 1996, 697–698.
35 A. Beeby, I. M. Clarkson, R. S. Dickins, S. Faulkner, D. Parker, L. Royle, S. A. S. de, J. A. G. Williams and M. Woods, *J. Chem. Soc., Perkin Trans. 2*, 1999, 493–504.
36 M. H. V. Werts, R. T. F. Jukes and J. W. Verhoeven, *Phys. Chem. Chem. Phys.*, 2002, **4**, 1542–1548.
37 K. Binnemans, *Coord. Chem. Rev.*, 2015, **295**, 1–45.
38 D. Kovacs, D. Kocsi, J. A. L. Wells, S. R. Kiraev and K. E. Borbas, *Dalton Trans.*, 2021, **50**, 4244–4254.
39 D. Kovacs, S. R. Kiraev, D. Phipps, A. Orthaber and K. E. Borbas, *Inorg. Chem.*, 2020, **59**, 106–117.
40 D. Kovacs, E. Mathieu, S. R. Kiraev, J. A. L. Wells, E. Demeyere, A. Sipos and K. E. Borbas, *J. Am. Chem. Soc.*, 2020, **142**, 13190–13200.
41 S. R. Kiraev, E. Mathieu, F. Siemens, D. Kovacs, E. Demeyere and K. E. Borbas, *Molecules*, 2020, **25**, 5282.
42 D. Kovacs, D. Phipps, A. Orthaber and K. E. Borbas, *Dalton Trans.*, 2018, **47**, 10702–10714.
43 D. Parker and J. A. G. Williams, *J. Chem. Soc., Perkin Trans. 2*, 1996, 1581–1586.
44 D. Kovacs and K. E. Borbas, *Coord. Chem. Rev.*, 2018, **364**, 1–9.
45 A. K. R. Junker and T. J. Sorensen, *Eur. J. Inorg. Chem.*, 2019, **2019**, 1201–1206.
46 L.-M. Fu, X.-C. Ai, M.-Y. Li, X.-F. Wen, R. Hao, Y.-S. Wu, Y. Wang and J.-P. Zhang, *J. Phys. Chem. A*, 2010, **114**, 4494–4500.
47 J.-C. G. Bunzli, *Coord. Chem. Rev.*, 2015, **293–294**, 19–47.
48 K. Suzuki, A. Kobayashi, S. Kaneko, K. Takehira, T. Yoshihara, H. Ishida, Y. Shiina, S. Oishi and S. Tobita, *Phys. Chem. Chem. Phys.*, 2009, **11**, 9850–9860.
49 A. Beeby, S. Faulkner and J. A. G. Williams, *J. Chem. Soc., Dalton Trans.*, 2002, 1918–1922.
50 S. V. Eliseeva, D. N. Pleshkov, K. A. Lyssenko, L. S. Lepnev, J.-C. G. Bunzli and N. P. Kuzmina, *Inorg. Chem.*, 2011, **50**, 5137–5144.
51 A. Beeby, D. Parker and J. A. G. Williams, *J. Chem. Soc., Perkin Trans. 2*, 1996, 1565–1580.